Seamless Physical-Layer Cross-Technology Communication from ZigBee to LoRa via Neural Networks

Demin Gao[®], Member, IEEE, Yongrui Chen[®], Member, IEEE, Ye Liu[®], Senior Member, IEEE, and Honggang Wang[®], Fellow, IEEE

Abstract—LoRa, designed for Low-Power, Wide-Area Networks (LPWANs), is widely used in the Internet of Things (IoT). In contrast, Wireless Personal Area Network (WPAN) technologies like ZigBee struggle to connect directly to LPWANs due to their limited communication range and differing modulation schemes. ZigBee uses Offset Quadrature Phase-Shift Keying (OQPSK) modulation, while LoRa employs Chirp Spread Spectrum (CSS) modulation, complicating cross-technology communication. To address this challenge, we propose a novel approach for seamless physical-layer cross-technology communication between ZigBee and LoRa networks, bridging the gap between short-range and long-range communication technologies. We introduce ZigRa, a communication method that leverages neural networks for efficient modulation translation between ZigBee's IEEE 802.15.4 standard and LoRa's CSS modulation. The core of ZigRa is a deep learning model that adapts and optimizes the transformation of ZigBee signals into ultra-narrowband single-tone sinusoidal signals, which can be reliably detected by LoRaWAN base stations. Our solution enables ZigBee devices to seamlessly connect to LoRa-based LPWANs, overcoming modulation mismatches and providing long-range connectivity. Extensive evaluations with both USRP hardware and commercial devices demonstrate that ZigRa achieves a frame reception rate exceeding 85% at distances up to 500 meters, significantly enhancing the interoperability and coverage of heterogeneous IoT networks.

Index Terms—Cross-Technology communication, LoRa, low-power wide-area networks, ZigBee.

Received 21 January 2025; revised 11 April 2025; accepted 11 June 2025. Date of publication 17 June 2025; date of current version 3 October 2025. This work was supported in part by Future Network Scientific Research Fund Project under Grant FNSRFP-2021-YB-17 and in part by The Priority Academic Program Development (PAPD) of Jiangsu Higher Education Institutions. An earlier version of this work has been accepted by the International Conference on Wireless Artificial Intelligent Computing Systems and Applications (WASA) 2024 [DOI: 10.1007/978-3-031-71464-1_10]. Recommended for acceptance by F. Wang. (Corresponding author: Ye Liu.)

Demin Gao is with the College of Information Science and Technology & Artificial Intelligence, Nanjing Forestry University, Nanjing 210037, China (e-mail: dmgao@njfu.edu.cn).

Yongrui Chen is with the School of Electronic, Electrical and Communication Engineering, University of Chinese Academy of Sciences, Beijing 100049, China (e-mail: chenyr@ucas.ac.cn).

Ye Liu and Honggang Wang are with the Department of Graduate Computer Science and Engineering, Katz School of Science and Health, Yeshiva University, New York, NY 10016 USA (e-mail: liuyefancy@gmail.com; Honggang.wang@yu.edu).

Digital Object Identifier 10.1109/TMC.2025.3580396

I. Introduction

N RECENT years, the demand for efficient communication in IoT has grown significantly, driven by the need for long-range, low-power wireless communication systems [2], [3], [4], [5], [6]. Technologies such as LoRa (Long Range [7]) and ZigBee have emerged as dominant solutions, each excelling in different aspects of wireless communication [8]. While LoRa is renowned for its long-range capabilities and robust signal transmission over large distances [9], ZigBee offers high data rates and low power consumption for short-range communications. However, the two technologies typically operate in isolated environments [10], with no seamless way to integrate them for improved performance across various ranges and data rate requirements.

The ability to combine the advantages of ZigBee and LoRa has the potential to transform the way IoT devices communicate by facilitating seamless CTC [11], [12]. This, however, presents a significant challenge, as the two technologies are fundamentally different in terms of modulation, signal processing, and operating conditions [13], [14]. A key obstacle lies in finding a practical and efficient method for transmitting ZigBee signals in a manner that LoRa receivers can interpret, thus enabling Physical-layer CTC (PHY-CTC) [15], [16], which in heterogeneous IoT refers to the ability of different systems to communicate and exchange data seamlessly, despite using different technologies, protocols, and standards [17]. The goal of CTC is to enable IoT devices from various vendors with differing capabilities can communicate and share information, thus providing a more comprehensive and integrated IoT solution [18]. For example, a device using the ZigBee protocol can directly communicate with another device using the LoRaWAN protocol. This capability allows a wide range of IoT devices to work together and share data, even though they use different communication technologies.

Despite recent advances in CTC techniques that offer new prospects for bridging the gap between ZigBee and LoRa, existing CTC methods fail to achieve directional communication from ZigBee to LoRa due to the inherent asymmetry in the CTC channel [19]. This has limited the practical deployment of such systems. For example, the research in BLE2LoRa [20], [21] focuses on finding a single-tone signal that exhibits clear signal characteristics in the LoRa frequency domain. Specifically, BLE2LoRa [20], [21] identifies only two symbols in the

1536-1233 © 2025 IEEE. All rights reserved, including rights for text and data mining, and training of artificial intelligence and similar technologies. Personal use is permitted, but republication/redistribution requires IEEE permission. See https://www.ieee.org/publications/rights/index.html for more information.

ZigBee signal, expressed as $e^{j2\pi ft}$ and $e^{-j2\pi ft}$. These represent a simplistic approach to signal mapping from ZigBee to LoRa. However, when LoRa receives the ZigBee signal, the LoRa device does not multiply it by a down-chirp, resulting in a limited and narrow solution.

In this article, we introduce a novel approach that addresses this challenge: Seamless physical-layer cross-technology communication from ZigBee to LoRa (called ZigRa) via Neural Networks, where we use machine learning, specifically neural networks, to facilitate the transformation of ZigBee signal characteristics into a format that is compatible with LoRa's CSS modulation. This enables LoRa receivers to decode ZigBee transmissions and effectively bridging the gap between the two technologies at the physical layer.

Our contributions are summarized as follows:

- We propose an innovative approach that leverages neural networks to bridge the physical-layer gap between ZigBee and LoRa by mapping ZigBee signals to ultra-narrowband single-tone sinusoidal signals required by LoRa receivers.
- We employ frequency peak positioning strategies to ensure robust separation and minimize interference by carefully designing the ZigBee sequences that their frequency peaks are separated from the LoRa signal's peaks.
- Extensive experiments were conducted using both universal software radio peripherals (USRP) hardware and commercial off-the-shelf devices. The experimental results show that ZigRa achieves a frame reception rate of over 85% at distances of up to 500 meters.

The structure of this paper is as follows. Section II presents the preliminaries. Section III provides the motivation for our research. Section IV gives an overview of ZigRa. Section V details our proposed system design. Section VI, we provide performance evaluation results for ZigRa. Section VII, we review previous research on CTC for heterogeneous IoT systems. Finally, Section VIII summarizes our conclusions and presents directions for future research.

II. PRELIMINARIES

A. OQPSK Modulation

The PHY layer of the ZigBee transceiver employs OQPSK, a digital modulation technique used in wireless communication [22]. It is a variant of QPSK, designed to reduce the peak-to-average power ratio of the transmitted signal. OQPSK encodes digital data onto a carrier signal by modulating both the amplitude and phase of the carrier signal. In OQPSK, similar to QPSK, the data stream s(k) is divided into two channels: the in-phase (I) and quadrature (Q). Specifically, two adjacent digital bits are mapped to the I-phase and Q-phase of the orthogonal carrier. Then, for each digital bit, a two-stage linear phase shift is applied. Since the two paths have a half-cycle offset, only one path can experience a polarity reversal at any one time. Consequently, the phase difference between adjacent orthogonal carriers is always 90°, 180°, or 270°. This mapping allows different digital bit sequences to be distinguished by varying phase differences, enabling the receiver to differentiate between data bits.

TABLE I KEY LORA PHYSICAL-LAYER PARAMETERS

Model Parameter	Symbol	Options
Frequency	F	2.4 GHz
Spreading factor	SF	5-12
Bandwidth	BW(kHz)	812, 1625
Code rate	CR	4/5
Cyclic Redundancy Check	CRC	on or of

B. CSS Modulation

Semtech's LoRa is a leading LPWAN technology that encompasses multiple wireless technologies and facilitates the development of scalable IoT networks. Within the unlicensed industrial, scientific, and medical (ISM) radio band, multiple wireless technologies, including IEEE 802.15.4 (e.g., ZigBee TI1352R [23]) and LoRaWAN (e.g., LoRa), coexist, especially in the Sub-1 GHz ISM band [24]. LoRaBee [25], [26] achieves data transmission from LoRa to ZigBee by embedding specific bytes into the payload of genuine LoRa packets and utilizing energy emission within the Sub-1 GHz bands. By leveraging, LoRaBee achieves a throughput of up to 281.61 bps.

Originally intended for Sub-1 GHz band operation, LoRa technology has incorporated 2.4 GHz LoRa transceivers since 2017, such as the SX1280/SX1281, which exhibit performance comparable to their Sub-1 GHz counterparts (i.e., 470-510 MHz for China, 433/868 MHz for the EU) [27]. Moreover, the SX1280 LoRa module has an extended communication range and is resistant to interference in this commonly used band, as shown in Table I. Additionally, it can receive LoRa packets without stringent duty cycle restrictions. At the same time, the maximum available bandwidth has been augmented from 500 kHz to 1600 kHz, resulting in faster data rates (i.e., from 21 kbps to 70 kbps). As a result, 2.4 GHz LoRa technology has garnered significant attention and offers broader support for IoT applications.

The use of chirp pulses in LoRa modulation enables efficient data transmission over long distances while maintaining low power consumption. Chirp signals are a type of continuous wave whose frequency varies linearly over time. This linear frequency variation results in a spread-spectrum signal that occupies a wide bandwidth. In LoRa, two different chirps are used to represent bit '0' and bit '1'. These chirps are then transmitted using frequency-shift keying (FSK) modulation [28], where the frequency of the transmitted signal alternates between the up-chirp and down-chirp frequencies.

III. MOTIVATION

A. Challenge

One of the key challenges in implementing ZigRa is the inherent complexity in training deep neural networks to model the mapping between two fundamentally different modulation schemes: ZigBee's Direct Sequence Spread Spectrum (DSSS) and LoRa's CSS. A particularly difficult aspect of this challenge is that LoRa's demodulation method is unique. When LoRa receives a time-domain waveform, it needs to multiply it by a falling edge before demodulating based on the frequency. This specialized demodulation technique makes it extremely

difficult to find a suitable ZigBee time-domain signal that aligns with LoRa's frequency-based demodulation requirements. The neural network must be trained to not only to translate the ZigBee signals into a format that can be interpreted by LoRa receivers but also account for this additional step in LoRa's signal processing. Achieving accurate signal conversion while respecting the intricacies of LoRa's demodulation process adds another layer of complexity to the solution.

Another challenge lies in the fact that the performance of the neural network heavily depends on the quality and diversity of the training dataset, which must cover a wide range of real-world conditions, including varying channel characteristics, interference levels, and noise types. Collecting and curating such a dataset for training can be both resource-intensive and time-consuming. Additionally, the real-time performance of the model can be affected by the computational complexity required for signal processing and mapping, especially in resource-constrained environments where power and processing capacity are limited. Achieving both high accuracy in signal translation and low latency for practical deployment remains a significant challenge.

B. Opportunity

The ZigRa framework presents several promising opportunities for advancing the interoperability of heterogeneous IoT networks. As IoT ecosystems continue to expand, the demand for communication solutions that seamlessly connect devices across different technologies-such as ZigBee, LoRa, and beyond-will only grow. ZigRa offers a unique opportunity to unify shortrange and long-range communication networks by bridging the gap between ZigBee and LoRa. This will enable devices in shortrange ZigBee networks to tap into the extensive coverage of LoRa networks, significantly enhancing the range and scalability of IoT deployments. The flexibility of neural network-based signal translation also opens up opportunities for future crosstechnology communication solutions, where new and emerging wireless standards can be integrated with minimal hardware changes, thereby reducing the time and cost required for IoT integration.

Furthermore, the use of machine learning, particularly neural networks, in cross-technology communication could pave the way for smarter and more adaptive IoT networks. By incorporating AI-driven algorithms, networks could dynamically optimize communication parameters based on environmental conditions and network load, thereby improving overall efficiency and reliability. ZigRa's approach also presents a clear pathway for future research in cross-technology communication, enabling the development of generalized models that could accommodate a wide range of modulation schemes and protocols. This adaptability can foster innovation in IoT applications, from smart cities to industrial automation, where seamless communication between a variety of devices, networks, and technologies is essential for efficient operation. As the demand for scalable, interoperable, and energy-efficient IoT networks grows, ZigRa's foundational approach can offer a solid framework for addressing these needs and expanding the possibilities of future IoT applications.

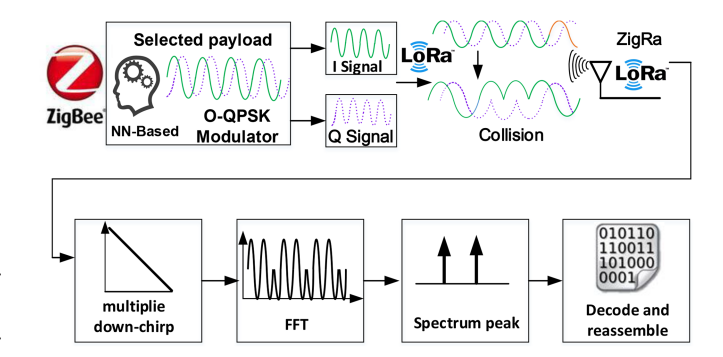


Fig. 1. Overview of ZigRa.

IV. ZIGRA IN A NUTSHELL

Fig. 1 depicts the ZigRa architecture and the data transmission process from a ZigBee device to a LoRa device. This process involves transmitting a ZigBee frame containing a chosen payload and generating a specific signal using OQPSK modulation. After receiving this signal, the LoRa device multiplies it by the down-chirp in the time domain (details are provided in Section II-A) and performs a Fast Fourier Transform (FFT) analysis. This analysis yields a detected peak in the frequency domain that corresponds to the ZigBee signal (assuming perfect synchronization). By detecting this peak, the base station can identify and track the ZigBee signal's bit stream, decode it, and reassemble it into ZigBee frames. This decoding process enables the LoRa device to extract the original payload data transmitted by the ZigBee device.

The key steps in this process include: i) ZigBee symbols are synchronized with the LoRa (Section V-A). ii) The neural network selects the most suitable payload by learning the relationship between the ZigBee signal and the LoRa demodulated signal (Section V-B and Section V-C). iii) Preamble detection for ZigRa (Section V-D). iv) LoRa receivers use the frequency-domain peak obtained from FFT demodulation to detect and decode the ZigBee signal (Section V-E). v) Configuration of ZigBee signals (Section V-F).

V. SYSTEM DESIGN

A. ZigBee Symbols are Synchronized With the LoRa

To accurately emulate the signals of ZigBee and LoRa devices through chirp emulation, it's crucial to carefully consider the inherent physical layer constraints of both technologies. Specifically, when emulating a chirp for transmission via ZigBee, it's essential to align the time duration of the emulated chirp with the characteristics of the target LoRa chirp. This necessitates a meticulous examination and synchronization of the time duration parameters within the chirp emulation process to faithfully replicate the behavior of LoRa chirps on authentic ZigBee and LoRa devices.

The chirp waveform, determined by a spreading factor (SF), consists of a total of 2^{SF} samples, maintaining a sampling rate equivalent to its bandwidth (BW). For instance, in a specific scenario where the spreading factor is designated as 7 and the bandwidth is $1625 \mathrm{kHz}$, the duration of the emulated chirp can

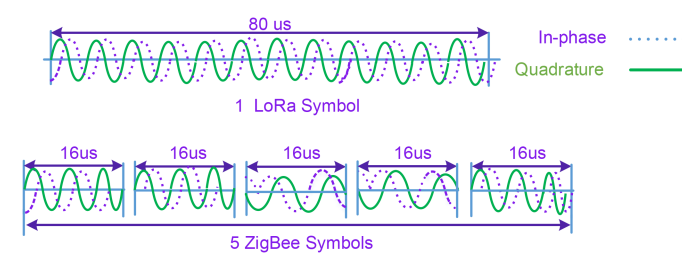


Fig. 2. ZigBee symbols synchronize with LoRa Symbol.

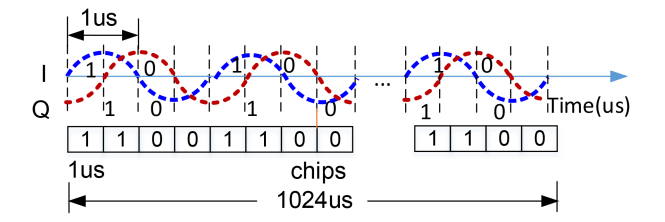


Fig. 3. Specific ZigBee waveforms utilized in ZigRa.

be computed as follows:

$$T_{symbol} = \frac{2^{SF}}{BW} = \frac{128}{1625KHz} \approx 80\mu s \tag{1}$$

The ZigBee (IEEE 802.15.4) device operates with a symbol duration of $16 \, \mu s$. To generate a waveform matching the duration of a single LoRa chirp, approximately 80/16 (that is, approximately 5) chips need to be transmitted. In the context of OQPSK modulation, each payload bit undergoes modulation into one OQPSK chip. Consequently, emulating a chirp waveform commonly employed in LoRa communication requires five ZigBee symbols. Thus, a complete LoRa symbol requires segmentation and emulation through five ZigBee symbols, as illustrated in Fig. 2.

B. Selecting ZigBee Waveforms for ZigRa

Building on the previous analysis of OQPSK and CSS, we explore the possibility of using specific ZigBee sequences to emulate LoRa signals. This process involves leveraging advanced neural networks to optimize waveform selection and ensure the successful decoding of ZigBee data by LoRa receivers. The ZigBee protocol is built on the IEEE 802.15.4 standard, which employs OQPSK modulation to encode data. This modulation scheme alternates between the I and Q components of the carrier signal. Specifically, the data bits are mapped to the I and Q components through the modulation of their phases. Each symbol represents a phase shift, with the values I and Q corresponding to specific binary sequences. For example, the chips c_0, c_2, \ldots are modulated onto the I signal, while the chips c_1, c_3, \ldots are modulated onto the Q signal, sequentially, as shown in Fig. 3.

In order to manipulate these signals for cross-technology communication, a numerically controlled oscillator (NCO) is employed. The NCO is a key component in both modulation and demodulation processes of digital communication systems. The NCO generates sinusoidal waveforms, which can be either

in-phase or quadrature, based on a phase control input. The phase of the NCO, denoted as ϕ , determines the output signal, which is typically expressed as $s=\sin(\phi)$ or $s=\cos(\phi)$. The phase ϕ can be expressed as:

$$\phi = f \cdot \omega \cdot t \tag{2}$$

where ω is the angular velocity, and f is the frequency of the signal. The relationship between angular velocity ω and frequency f is given by $\omega = 2\pi f$. Therefore, at any given time t, the signal can be expressed as:

$$s(t) = \sin(2\pi ft) \quad \text{or} \quad s(t) = \cos(2\pi ft) \tag{3}$$

This mathematical model enables the generation of both sine and cosine signals, which are essential for modulating the *I* and *Q* components. In ZigRa, the goal is to select specific ZigBee waveforms that can be mapped to LoRa symbols in such a way that ensures the successful transmission and decoding of data. To achieve this, we need to align the frequency characteristics of the two systems. Specifically, the goal is to map ZigBee bit sequences to the 128 LoRa symbols generated during one symbol duration. Let us consider the modulation of ZigBee signals using a binary pattern of '1010...' applied to the *I*-channel chips and '1010...' applied to the *Q*-channel chips. The resulting waveform forms a complex exponential signal, which can be expressed in terms of real and imaginary components as:

$$e^{j(2\pi ft + \psi)} = \cos(2\pi ft + \psi) + j\sin(2\pi ft + \varphi) \qquad (4)$$

Here, ψ and φ represent phase shifts for the in-phase and quadrature components, respectively. The phase and frequency of the generated signal are directly tied to the chip patterns being used. To encode a LoRa symbol, a sequence of ZigBee bits is necessary. As an example, it takes a total of 180 bits, derived from the pattern '1100 1100... 1100', to encode one LoRa symbol, with the symbol duration approximately equal to $80~\mu s$ (as discussed in Section V-A). This means that each LoRa symbol is represented by a specific set of ZigBee waveforms that correspond to a certain group of bits.

Now, we need to ensure that the selected ZigBee waveforms are compatible with the LoRa system for successful communication. LoRa utilizes CSS modulation, where each symbol is spread across 2^{SF} chip sequences, where SF represents the spreading factor. When the spreading factor SF is set to 7, there are 128 distinct chip sequences, each corresponding to a unique LoRa symbol. These sequences are generated by applying a frequency shift to the base frequency, and the frequency difference of each sequence can be expressed as:

$$f_{\text{init}}(k) = \frac{BW \times k}{2^{SF}}, \quad k \in [0, 2^{SF} - 1]$$
 (5)

where BW is the bandwidth of the system, and k represents the index of each chip sequence. For each k, the corresponding initial frequency $f_{\rm init}(k)$ is different, and this variation allows the frequency space to be divided into 2^{SF} unique sequences. The challenge in ZigRa is to map the 128 distinct ZigBee waveforms to the 128 different LoRa chip sequences such that the resulting signal is compatible with LoRa's CSS modulation. This requires careful selection of ZigBee waveforms, as each LoRa symbol

must be represented by a unique pattern of ZigBee bits. This task is computationally complex due to the large number of possible ZigBee bit sequences, specifically 2^{80} possible combinations for a single LoRa symbol. Our ultimate goal is to find a bit sequence out of 2^{80} in the ZigBee domain, which can be mapped to a bit sequence out of 2^{7} in the LoRa domain. Formally, the mapping is defined as follows:

$$P_{ZigBee} \in \mathcal{P}_{ZigBee}^{2^{80}} \mapsto P_{LoRa} \in \mathcal{P}_{LoRa}^{2^7} \tag{6}$$

where \mathcal{P} denotes the value space. Finding a particular map for a given P_{LoRa} by brute force is harder than looking for a needle in a haystack because the combinations are more than the number of atoms in the universe. To handle this complexity, ZigRa employs neural network-based algorithms for waveform selection. The neural network is trained to optimize the mapping between ZigBee sequences and LoRa symbols by learning the underlying relationships between the two systems. The training process involves using a dataset that contains pairs of ZigBee waveforms and their corresponding LoRa symbols.

By minimizing the error between the predicted and actual LoRa symbols, the neural network learns to identify the optimal ZigBee waveforms that can be used for each LoRa symbol. Once trained, the neural network can quickly identify the most suitable ZigBee waveforms for any given LoRa symbol, ensuring that the data can be transmitted efficiently and decoded accurately by LoRa receivers. This approach significantly reduces the complexity of waveform selection compared to traditional methods, where exhaustive search or manual mapping would be required (The detail is shown in Section V-C).

C. ZigRa Based on Neural Network

At the heart of the waveform-emulated ZigRa framework is the complex task of identifying ZigBee payloads that can replicate the waveform of specified LoRa packets. Traditional methods in CTC systems have often relied on reverse engineering to achieve this goal. In conventional CTC systems, the goal is to transmit a packet P_{LoRa} from a LoRa sender to a LoRa receiver over a ZigBee channel. Reverse engineering is employed to determine the appropriate payload P_{ZigBee} capable of generating a waveform similar to the desired P_{LoRa} , thereby allowing LoRa receivers to decode the transmitted message accurately.

In our system, the transformer model receives as input a fixed-length binary sequence derived directly from the ZigBee payload. We emphasize that the transformer does *not* operate on raw I/Q samples. Instead, we adopt a lightweight symbolic-level input representation that facilitates real-time compatibility with ZigBee hardware constraints. Let $\mathbf{x} = [x_1, x_2, \ldots, x_n]$ denote the ZigBee payload bits, where each $x_i \in \{0, 1\}$. The input feature space is defined as:

$$\mathcal{X} = \left\{ \mathbf{x} \in \{0, 1\}^n \mid n = \frac{T_{\text{symbol}}}{T_{\text{bit}}} \right\} \tag{7}$$

where $T_{\rm symbol}$ denotes the LoRa symbol duration (e.g., $80~\mu s$ for SF=7 and BW=1625 kHz), and $T_{\rm bit}$ is the ZigBee bit duration



Fig. 4. In order to access food while avoiding competition with other herbivores, giraffes gradually evolved their remarkable long necks. This adaptation allows them to easily feed on the leaves and branches at the top of trees, which are otherwise out of reach for most other animals.

 $(1 \mu s)$. Therefore, each LoRa symbol interval corresponds to n=80 ZigBee bits, forming the transformer's input vector.

ZigBee symbols are mapped to OQPSK waveforms according to the IEEE 802.15.4 standard, where each 4-bit symbol is spread into a 32-chip pseudo-random (PN) sequence. Chips are interleaved into I and Q streams with a half-symbol delay. In our model, we treat this modulation pipeline as a fixed deterministic mapping. Phase ambiguities inherent in OQPSK are resolved by assuming a consistent initial phase reference across the training dataset, ensuring stable waveform semantics. The neural network thus implicitly learns to account for such phase relationships during training. The model learns a mapping function:

$$\mathcal{F}: \{0,1\}^n \to \mathbb{R}^{128} \tag{8}$$

which predicts the frequency-domain energy distribution across FFT bins (128 bins for SF=7). The target is the FFT bin index k^* corresponding to the peak detected at the LoRa receiver after demodulation. Training samples are constructed using empirical waveform transmission over the air, where each ZigBee payload x is paired with its resulting FFT peak index observed by a LoRa receiver. This representation avoids the need for real-time signal synthesis and enables efficient and practical payload selection on constrained ZigBee devices.

In the context of communication, the relationship between ZigBee and LoRa can be likened to a linguistic analogy in natural languages, specifically the phenomenon of homophony. Homophony occurs when words from different languages have the same or nearly identical pronunciation, despite differing meanings or etymologies. A classic example of homophony is found in the Chinese phrase 'san ke you,' which closely resembles the English expression 'thank you' in pronunciation, albeit with a different meaning. This analogy serves as a practical illustration of how seemingly disparate systems, like ZigBee and LoRa, can share waveform characteristics, even though their underlying technologies are vastly different.

This cross-linguistic homophony phenomenon has practical applications in translating foreign product brands. Brands often use homophonic phrases from other languages to create names that sound similar to their original counterparts, despite the languages being linguistically distinct. This concept, depicted in Fig. 4, reflects how ZigBee can generate waveforms that emulate those of LoRa, even though the two technologies operate on different modulation schemes.

Inspired by this linguistic analogy, we introduce NN-ZigRa (ZigRa based on Neural Network), an innovative solution designed to facilitate waveform-emulated CTC between ZigBee and various LoRa devices. NN-ZigRa leverages a Neural Network-based CTC framework to achieve this complex task. In this study, we redefine CTC as a classical language translation problem, which aligns with the domain of neural language processing, where significant advancements have been made in recent years. The application of neural networks to CTC challenges is particularly powerful in addressing complex, nonlinear relationships between different modulation schemes, such as ZigBee's OQPSK and LoRa's CSS.

The neural network model used in ZigRa is designed to optimize the mapping between ZigBee waveforms and LoRa symbols. The input to the network consists of ZigBee bit sequences, while the output is the corresponding LoRa symbol. This procedure treats the ZigBee sender and LoRa receiver as functionally abstracted modules, without relying on the knowledge of their internal implementation details. It repeats until a sufficient number of pairs are found. The procedure proceeds from the ZigBee sender to the LoRa receiver. It aims to pick a small percent of the mappings from the almost infinitely possible pairs. Let $X = \{x_1, x_2, \ldots, x_n\}$ represent a set of ZigBee sequences, where each x_i is a sequence of bits mapped to the I and Q components. The network learns a mapping $f(X) \to Y$, where Y represents the LoRa symbol corresponding to the ZigBee bit sequence. The loss function for training is defined as:

$$L = \sum_{i=1}^{n} ||f(x_i) - y_i||^2$$
(9)

where y_i represents the target LoRa symbol, and $\|\cdot\|$ denotes the Euclidean distance between the predicted and actual LoRa symbols. The network is trained to minimize this loss, ensuring that the predicted symbols are as close as possible to the true LoRa symbols. Once trained, the neural network can be used to predict the appropriate ZigBee waveforms for any LoRa symbol, making the waveform selection process efficient and scalable.

NN-ZigRa is not limited to ZigBee and LoRa communication but is adaptable to a range of CTC applications across diverse protocols that operate within the same spectrum. The model is designed to be extensible, meaning it can be applied to any pair of communication technologies that require waveform translation. NN-ZigRa adopts a holistic approach to CTC by treating communication devices and channels as black boxes. This enables the system to emulate the waveform of any desired LoRa packet from a given ZigBee payload without requiring detailed knowledge of the internal workings of the devices or channels. The architectural layout of NN-ZigRa is illustrated in Fig. 5, providing a visual representation of how the system is structured.

At the core of NN-ZigRa's functionality is the critical role played by the training dataset. Building an extensive and accurate repository of ZigBee-to-LoRa mappings is essential to the success of the neural network model. The dataset must cover a wide range of ZigBee payloads and their corresponding LoRa packets, ensuring that the generated waveforms exhibit a high

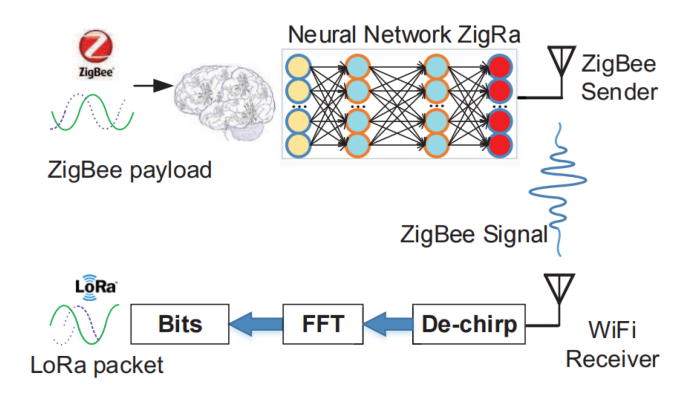


Fig. 5. The architecture of NN-ZigRa.

degree of similarity to the desired LoRa signals. This process requires careful attention to the characteristics of both ZigBee and LoRa modulation schemes.

A key challenge lies in the fact that LoRa symbols persist for 80 μs , whereas a ZigBee symbol, which represents 4 bits, lasts for only 16 μs . More specifically, each ZigBee symbol lasts for 4 μs , and each ZigBee bit lasts for 1 μs . These time differences pose a significant challenge when attempting to align ZigBee signals with LoRa signals, as there is a large discrepancy between the symbol durations of the two technologies. However, within the 80 μs duration of a LoRa symbol, there is sufficient time to transmit 80 ZigBee bits, which can be used to emulate the waveform of a LoRa packet. This results in a pool of 2^{80} potential ZigBee bit sequences from which the optimal sequence must be selected.

The primary objective of NN-ZigRa is to identify the appropriate bit sequence from the ZigBee domain that can emulate the waveform characteristics of a LoRa packet. To achieve this, we employ a training methodology that allows the neural network to learn the best possible mapping between ZigBee payloads and LoRa packets. This involves training the network to discern the patterns in the ZigBee signals that most closely match the waveforms required for LoRa reception.

To accomplish the complex task of mapping ZigBee payloads to LoRa waveforms, we employ a transformer neural network architecture, which has gained prominence in sequence-to-sequence translation tasks. The Transformer architecture excels in handling long-range dependencies and captures contextual information from the input sequence through a self-attention mechanism. This mechanism allows the model to dynamically focus on different parts of the input sequence during the encoding process, thereby enhancing the model's ability to capture important features of the signal. The Transformer's self-attention mechanism can be expressed as follows:

$$Attention(Q, K, V) = softmax\left(\frac{QK^T}{\sqrt{d_k}}\right)V \qquad (10)$$

where Q is the query matrix, K is the key matrix, V is the value matrix, and d_k is the dimension of the key vector. The self-attention mechanism allows the model to determine which parts of the input sequence are most relevant to a given output. In the context of ZigBee-to-LoRa translation, the self-attention mechanism helps the network focus on specific ZigBee bits

that are most relevant for generating the corresponding LoRa symbol.

The transformer model consists of an encoder-decoder structure, where the encoder processes the input ZigBee bit sequence and the decoder generates the corresponding LoRa symbol. The encoder-decoder architecture enables the model to perform efficient sequence-to-sequence translation, which is crucial for waveform emulation. Specifically, the encoder converts the input ZigBee signal into a higher-dimensional representation, and the decoder maps this representation to a LoRa waveform.

During training, the NN-ZigRa model learns the optimal transformation from ZigBee bit sequences to LoRa waveforms by minimizing the error between the predicted LoRa signal and the actual LoRa waveform. This training process is guided by a loss function that quantifies the difference between the predicted waveform and the target waveform. A common loss function for regression tasks, such as this one, is the mean squared error (MSE) loss:

$$L(\theta) = \frac{1}{N} \sum_{i=1}^{N} (y_i - \hat{y}_i)^2$$
 (11)

where y_i represents the true LoRa symbol, \hat{y}_i represents the predicted LoRa symbol, and N is the total number of samples in the dataset. The loss function provides a measure of how well the network is performing and guides the optimization of the model's parameters. LoRa demodulation produces discrete FFT peak indices, which makes this appear to be a classification task. In conventional classification problems, cross-entropy loss is appropriate when: The output is categorical (e.g., class indices) and the model produces a probability distribution over the classes (e.g., softmax). However, in ZigRa, the FFT peak index is treated as a continuous frequency-domain position. Due to frequency offset, symbol drift, and neural waveform mismatches, the resulting FFT bin may lie near-but not exactly at-the intended bin. Thus, treating this as a strict classification task could penalize small misalignments disproportionately.

Once the NN-ZigRa model has been trained, it can generate a ZigBee bit sequence that produces a waveform suitable for LoRa reception. This process involves two key steps: The trained model takes a ZigBee payload as input and generates a corresponding LoRa waveform. The waveform is generated by passing the input ZigBee sequence through the transformer model, which encodes the ZigBee bits into a latent space representation and decodes it into a LoRa signal. After the time-domain waveform is generated, it is multiplied by a down-chirp signal, which is characteristic of LoRa's CSS modulation. This operation shifts the frequency of the waveform into the appropriate frequency domain, allowing it to be processed by a LoRa receiver. The resulting signal can then be demodulated using the LoRa receiver's frequency-domain processing techniques.

Despite the unique challenges posed by LoRa's modulation technique, the neural network model proves effective in generating time-domain waveforms that align with LoRa's reception characteristics. This demonstrates the feasibility of using neural networks for cross-technology waveform simulation, although implementing such a system in practice requires rigorous validation of the model's performance across various scenarios.

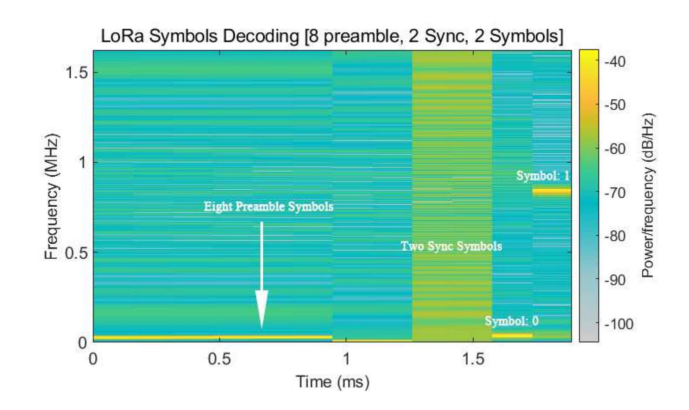


Fig. 6. LoRa decoded symbols.

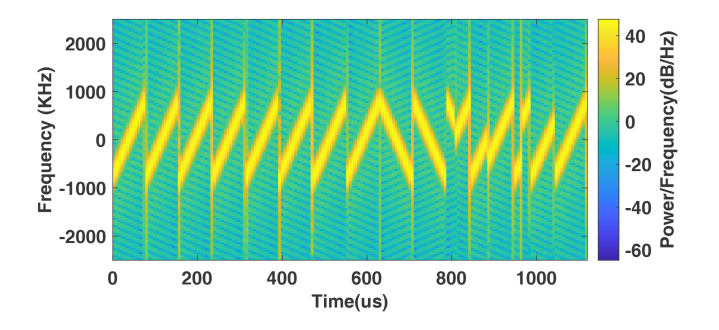


Fig. 7. LoRa Signal Structure, including the preamble, sync word, start frame delimiter, and payload.

D. Preamble Detection

The preamble plays a critical role in enabling the receiver to synchronize with the transmitter in terms of frequency and timing. This synchronization allows the receiver to establish and maintain a stable connection with the transmitted signal. Additionally, the preamble allows the receiver to distinguish the beginning of the transmission from other signals or noise present on the same frequency. The receiver initiates the demodulation process by extracting the chirp signal embedded within the received signal. Once the chirp signal is extracted, the receiver applies the inverse chirp to convert it back to its original data signal. During the decoding of message symbols, symbols representing '0' may resemble the symbols used in the preamble. Conversely, for symbols representing '1', the starting frequency is precisely positioned at the midpoint, as illustrated in Fig. 6.

Fig. 7 illustrates the LoRa symbols (preamble, sync word, start frame delimiter, and payload). The preamble serves as a standardized pre-transmission sequence typically transmitted prior to the actual data payload. The LoRa preamble comprises three primary components: a variable preamble, a sync word, and a start frame delimiter (SFD). The variable preamble, typically consisting of multiple up-chirp symbols, serves various purposes such as signal detection, receiver gain configuration, and frequency and sampling time synchronization. Its length is determined by the chip's registers and is commonly set to 6 symbols. The sync word, occupying a field of 2 symbols, enables quick identification of distinct LoRa networks, helping distinguish between different network environments. The SFD, a standardized down-chirp signal lasting 2.25 symbols,

signals the end of the preamble and the start of data payload transmission, facilitating accurate parsing of the transmitted data by the receiver.

It is interesting to note that ZigRa incorporates a robust preamble detection and synchronization strategy that enables LoRa receivers to detect and align with the beginning of the ZigBee-emulated waveform. As detailed in Section V-D and V-E, ZigRa inserts a specifically designed preamble at the start of transmission, which, after multiplication by a down-chirp and FFT processing, yields clearly identifiable frequency peaks. These peaks serve as markers for frame alignment and compensate for minor timing offsets by allowing the receiver to realign with the signal's FFT window. This mechanism is similar to traditional LoRa preamble-based synchronization.

ZigRa uses the standard LoRa CRC mechanism at the receiver, which is preserved throughout the ZigRa data path. After the frequency-domain peak detection and symbol reassembly, the reconstructed ZigBee payload is passed through CRC validation. Packets that fail CRC checks are discarded, which helps mitigate FFT misalignment-induced errors. While ZigRa currently implements a basic CRC-based discard mechanism, retransmission support is compatible with existing ZigBee MAC-layer ACK and retry mechanisms. In practical deployments, MAC-layer retransmissions can be used to improve reliability without any modification to the LoRa receiver.

E. ZigRa Demodulation

The demodulation process in ZigRa involves several key steps that ensure the reliable extraction of ZigBee data from a signal modulated using LoRa's CSS. The process can be broken down into clear stages: waveform identification, correlation with the reference template, signal down-chirp multiplication, frequency analysis, preamble detection, and final bit demodulation. These stages are described in more detail below, along with the necessary mathematical background.

Once the transmitted waveform is selected, ZigRa uses a correlation template to detect the signal segment. The correlation template serves as a reference that ZigRa compares with the received signal to detect the presence of the expected waveform. This step is essential for distinguishing the desired ZigBee signal from noise or interference that may be present. The correlation between the received signal r(t) and the template t(t) is expressed as:

$$C(\tau) = \int_{-\infty}^{\infty} r(t) \cdot t(t - \tau) dt$$
 (12)

where τ is the time lag of the correlation. A peak in the correlation output indicates the position of the waveform in the received signal. Once the correct segment of the signal is identified, ZigRa multiplies the signal by a down-chirp in the time domain. The down-chirp is used to reverse the frequency shift introduced by LoRa's CSS modulation. This process shifts the frequency components of the signal, bringing them to the baseband, which facilitates easier demodulation. The down-chirp multiplication is expressed mathematically as:

$$r_{\text{chirped}}(t) = r(t) \cdot e^{-j2\pi f_{\text{chirp}}t}$$
 (13)

where $f_{\rm chirp}$ is the chirp rate. This multiplication effectively reverses the frequency modulation applied by the LoRa transmitter, making it easier for ZigRa to detect the underlying ZigBee signal. After the signal is down-chirped, ZigRa performs a FFT on the signal. The FFT decomposes the signal into its frequency components, revealing peaks at specific frequencies that correspond to the encoded symbols. The frequency resolution $f_{\rm res}$ of the FFT is determined by the time window T used for the analysis, $f_{\rm res}=1/T$.

In the case of ZigRa, if the time window T is set to $80~\mu s$ (as typical for ZigBee signals), the frequency resolution will be: $f_{\rm res}=1/80\mu s=12.5\,{\rm kHz}$. This resolution allows ZigRa to differentiate the ZigBee signal peaks, which are located at $\pm 500\,{\rm kHz}$, giving the peaks at positions: $\pm 500/12.5=\pm 40$. ZigRa detects the preamble of a ZigBee frame by identifying a series of repeated frequency peaks, which indicate the start of the frame. These peaks are periodic and allow ZigRa to synchronize with the incoming signal. The preamble provides a clear marker for the beginning of the transmission, enabling ZigRa to lock onto the signal and extract the subsequent data correctly.

Once the preamble is detected, ZigRa traces the corresponding peaks to demodulate them into symbols or bits in parallel. This process involves converting the analog signal into a digital form. The demodulated bits are then packed into frames. ZigRa uses the known properties of ZigBee modulation to accurately recover the bitstream, enabling reliable data transmission. The demodulated bits b are packed into frames F, as follows:

$$F = \{b_1, b_2, \dots, b_n\} \tag{14}$$

where b_i represents each demodulated bit. In ZigRa, ZigBee and LoRa operate at different frequencies, making it possible to distinguish their signals based on their frequency components. The frequency deviation of the ZigBee waveform is $\pm 500\,\mathrm{kHz}$, corresponding to a tone period of 2 $\mu\mathrm{s}$, as shown in Fig. 3. ZigRa capitalizes on this frequency difference to separate the two signals.

In contrast, for a LoRa symbol, the number of peak locations in the FFT depends on the symbol cardinality. For example, if each LoRa symbol corresponds to two bits, the peaks will have specific locations such as the 0th, 32nd, 64th, and 96th bins in the FFT (assuming an FFT size of 128). These locations are fixed and do not overlap with the ZigBee peaks, making it easy for ZigRa to distinguish between the two signals. Fig. 8 illustrates the clear separation between ZigBee and LoRa peaks. These steps allow ZigRa to isolate and successfully demodulate ZigBee frames, enabling efficient and reliable communication in environments where ZigBee and LoRa signals coexist.

ZigRa relies on selecting specific ZigBee sequences to generate frequency peaks that are compatible with LoRa's CSS. The fundamental goal of this approach is to create distinct frequency components for ZigBee signals that can be demodulated even when they coexist with LoRa signals. However, the peak value of the LoRa signal at the receiver is uncontrollable, and this can lead to situations where the ZigBee and LoRa signals overlap in the frequency domain, potentially causing interference if they share the same frequency peak. To address this concern, we employ frequency peak positioning strategies in the ZigRa system to

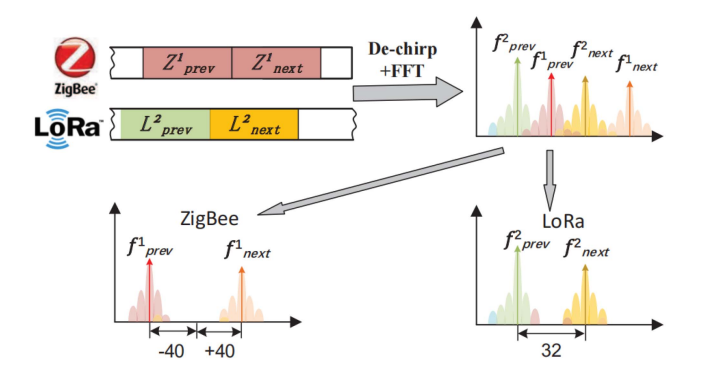


Fig. 8. Distinguishable collision of ZigBee and LoRa.

ensure robust separation and minimize interference. The key idea behind the ZigRa system is to carefully design the ZigBee sequences to ensure that their frequency peaks are separated from the LoRa signal's peaks in the frequency domain. However, since LoRa's signal peaks are determined by the SF and the frequency offset, the overlap of ZigBee and LoRa peaks may still occur under certain conditions.

We use a dynamic frequency adjustment strategy in which ZigRa can adjust the frequency range of ZigBee sequences to avoid overlap with the LoRa signal peaks. This flexibility allows the system to adapt to the frequency characteristics of the LoRa signal in real-time, reducing the likelihood of peak overlap. The neural network used in ZigRa plays a crucial role in optimizing the mapping of ZigBee sequences to LoRa-like frequency peaks. The network is trained to identify and mitigate potential conflicts by ensuring that the mapped ZigBee sequences are placed in frequency bins that minimize the impact of interference from LoRa. When ZigBee and LoRa signals overlap at the same frequency peak, we employ interference cancellation techniques in the receiver.

The receiver is designed to detect and isolate peaks by first identifying distinct frequency patterns associated with ZigBee and LoRa signals. Even if the signals overlap at the same frequency, the modulation characteristics (e.g., phase shifts, spreading factors) of each signal differ, allowing the receiver to distinguish between them. If overlapping peaks are detected, ZigRa uses signal reconstruction algorithms to separate the components of the ZigBee and LoRa signals. This involves processing the signal in the time domain after down-chirping to reconstruct the individual signal components. In some cases, weighted filtering techniques can be applied to prioritize the ZigBee signal in the presence of LoRa interference, based on the known characteristics of both signals. This helps reduce the impact of the LoRa signal on the ZigBee demodulation process.

F. Configuration of ZigBee Signals

In ZigBee wireless communication, the default configuration utilizes a technique called DSSS to spread a ZigBee symbol, comprising four bits, into a predefined 32-chip sequence known as the Pseudo-Noise (PN) sequence. However, due to the predefined nature of the PN sequence utilized in DSSS, it's not feasible to arbitrarily select the chips to generate desired signals,

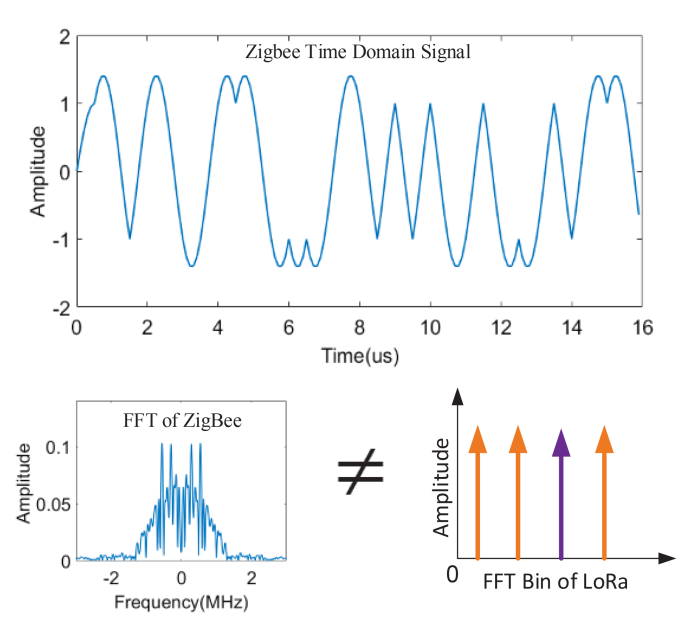


Fig. 9. ZigBee simulation timing waveform diagram for symbol '0' based on DSSS, which do not meet the needs of generating special LoRa Waveforms.

as illustrated in Fig. 9. This implies that the selection of the PN sequence and its corresponding chips are crucial for achieving the desired signal characteristics. In DSSS, the spreading of the ZigBee symbol into the 32-chip PN sequence aids in spreading the signal across a wide frequency band. This spread contributes to robustness against narrow-band interference and noise. Subsequently, the receiver despreads the received signal using the same PN sequence, thereby enhancing the signal-to-noise ratio and mitigating the effects of interference.

The default configuration of ZigBee employs DSSS to expand a four-bit ZigBee symbol into a predefined 32-chip PN sequence. While PN sequences offer robustness against interference and noise, they limit the ability to select arbitrary chips for signal generation. However, the IEEE 802.15.4 g standard specifies that commodity ZigBee radio chips, such as Atmel AT86RF233 and Atmel AT86RF215, can support versatile data rates ranging from 250 kb/s to 2000 kb/s by adjusting the spreading factors in DSSS

Long-range communication waveforms for ZigBee can be generated by selecting the payload bits of the ZigBee frame. This approach enables the implementation of an ultra-low-cost payload encoding method, facilitating ubiquitous LPWAN without requiring any hardware modifications to existing IoT devices. Such an approach offers a cost-effective solution for enabling long-range communication, particularly for resource-constrained IoT devices that require energy-efficient communication methods.

G. Long Range Communication for ZigRa

In the realm of wireless communication, achieving long-range transmission typically involves increasing transmission power, improving receiver sensitivity, or a combination of both. LoRa, a wireless communication technology, focuses on enhancing receiver sensitivity, boasting an impressive sensitivity of up to

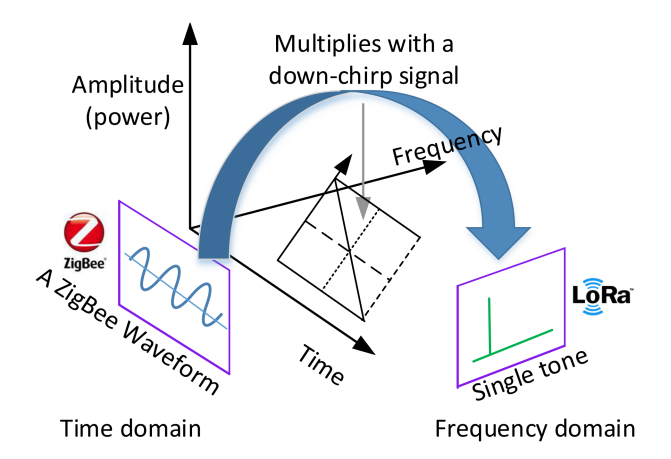


Fig. 10. Modulation process and format IEEE 802.15.4-2006 symbol to chip mapping, where a sequences '1100 1100... 1100' to encode a LoRa symbol.

-134 dBm. This exceptional sensitivity is a result of LoRa's utilization of spread-spectrum techniques, particularly CSS, a core feature of LoRa.

CSS involves expanding a narrow-band signal into a wide-band transmission, enabling it to travel extended distances with-out significant signal attenuation. Upon reaching the receiver, the wide-band transmission undergoes template correlation, which reverts the signal back to its original narrow-band form. This process effectively spreads both narrow-band interference and noise across a wide bandwidth, allowing for differentiation using FFT. As a result, the energy of the original signal becomes concentrated in a narrow bandwidth, making it distinguishable from the widespread energy of noise and interference. Hence, LoRa's utilization of CSS significantly contributes to its high receiver sensitivity, enabling robust long-range wireless communication.

In contrast, ZigBee achieves long-range communication through the use of specific waveforms optimized for extended-distance transmission. These waveforms generate ultranarrowband signals resistant to interference and noise, easily detected and demodulated even under challenging signal conditions. During a FFT time window equivalent to the duration of a clear to send symbol, the specific waveform produces a single-tone sine wave that is ultra-narrowband. Consequently, the signal energy is concentrated within a narrow frequency band, facilitating its distinction from noise and interference. ZigRa emulates the frequency-domain footprint of LoRa chirps rather than transmitting actual wideband chirps. By leveraging carefully selected ZigBee payloads that produce narrowband tones, ZigRa allows the LoRa receiver to detect symbols in the FFT domain similarly to how it would process real chirps.

VI. PERFORMANCE EVALUATION

We will now present empirical results for the generalized ZigRa framework and provide a detailed account of the experimental setup.

A. Hardware

Fig. 11 illustrates the experimental setup of the ZigRa system. Implemented on the USRP (Universal Software Radio



Fig. 11. Experimental Testbed of ZigRa.

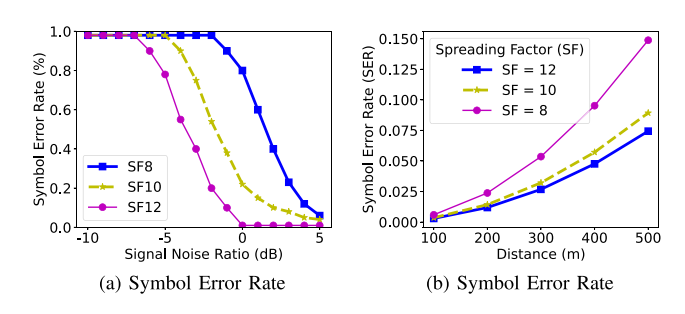


Fig. 12. Symbol error rate comparison for ZigRa with different SF configurations and various SNRs and distances. (a) Symbol Error Rate. (b) Symbol Error Rate

Peripheral) B210 platform with LoRa PHY [29], the ZigRa sender (i.e., ZigBee) operates on commercial chips, specifically the Atmel AT86RF233 compliant with the IEEE 802.15.4 g standard. The transmission power of the ZigRa sender is set to 0 dBm by default. On the receiving end, the ZigRa receiver (i.e., LoRa receiver) utilizes a Semtech SX1280 chip, employing a bandwidth of 812 KHz and a spreading factor of 8, with the channel frequency set at 2.4 GHz. Demodulation and decoding of ZigBee signals are performed using LoRa and USRP-B210 devices at the receiver. The commercial ZigBee and LoRa devices are used to simulate real-world deployment conditions. The USRP is used for LoRa PHY implementation and custom signal processing, offering flexibility for experimentation. The combination of these two types of devices ensures that the system is both flexible for research purposes and compatible with commercial systems.

B. Experimental Insight

Fig. 12 shows the performance of ZigRa with different SFs and signal-to-noise ratios (SNRs) for a BW of 812 KHz. Higher SFs result in better performance for ZigRa, attributed to longer chirp lengths that concentrate signal energy during demodulation. As depicted in Fig. 12(a), the symbol error rates (SERs) of ZigRa increase with decreasing LoRa SNR. However, compared to other systems, ZigRa exhibits a slower increase in SER. Even under challenging conditions where the signal power is weaker than the noise (SNR < 0), ZigRa maintains a relatively low SER.

Fig. 12(b) illustrates the SER as a function of distance for different SF values: 8, 10, and 12. As the SF increases, the SER

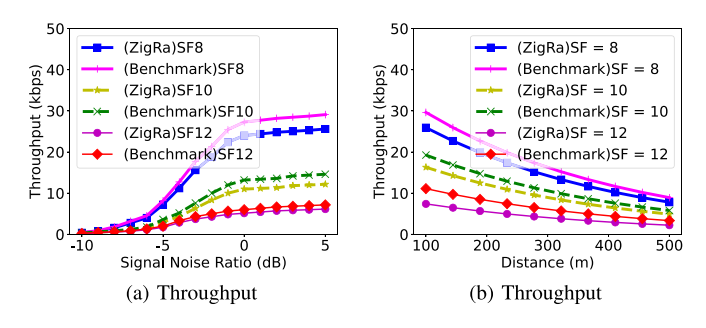


Fig. 13. Throughput comparison for ZigRa with different SF configurations and various SNRs and distances. (a) Throughput. (b) Throughput.

decreases. This is because a higher SF improves the robustness of the communication system, making it less susceptible to errors. In this case, SF = 12 shows the lowest SER, followed by SF = 10, and SF = 8 shows the highest SER. As the distance increases, the SER increases, which is expected because the signal power weakens with distance due to the inverse square law. This leads to a lower SNR, which results in a higher error rate. The curves for each SF are upward sloping, indicating that as the distance increases, the Symbol Error Rate increases, which aligns with the expected physical behavior of wireless communication systems.

The remarkable performance of ZigRa can be attributed to its utilization of chirp de-spreading, effectively concentrating energy and enhancing noise immunity for long-range transmissions. This feature enables ZigRa to maintain reliable communication even amidst significant signal attenuation during propagation. Fig. 13(a) represents the throughput of two systems, ZigRa and a benchmark, at different SNRs and for various SF. Specifically, the plot compares ZigRa's performance at spreading factors SF=8, SF=10, and SF=12 with the benchmark system operating at the same spreading factors.

As the SNR increases, the throughput for both ZigRa and the benchmark system improves. However, ZigRa consistently performs better than the benchmark across all SNR levels for the same spreading factors. For both ZigRa and the benchmark system, the throughput increases as the spreading factor decreases. This is because lower SF values allow for faster transmission, but at the cost of reduced range and robustness to noise. Specifically, SF=8 offers the highest throughput, while SF=12 provides the lowest throughput but the greatest resilience to noise. For ZigRa, the throughput at SF=8 starts to plateau at higher SNR values, while for the benchmark system, the throughput continues to increase gradually. This suggests that ZigRa has a more efficient method of utilizing the available bandwidth and achieving high throughput in high SNR conditions.

Fig. 13(b) the Throughput as a function of distance for three different SF: 8, 10, and 12 for both ZigRa and Benchmark systems. As the distance increases, the throughput decreases for all SF. This is because longer distances result in greater signal attenuation, which reduces the ability to maintain a high data rate. The exponential decay curve in each plot shows how the throughput diminishes as distance increases. ZigRa (SF=8) shows the highest throughput, followed by ZigRa (SF=10) and ZigRa (SF=12). This suggests that ZigRa with lower SF

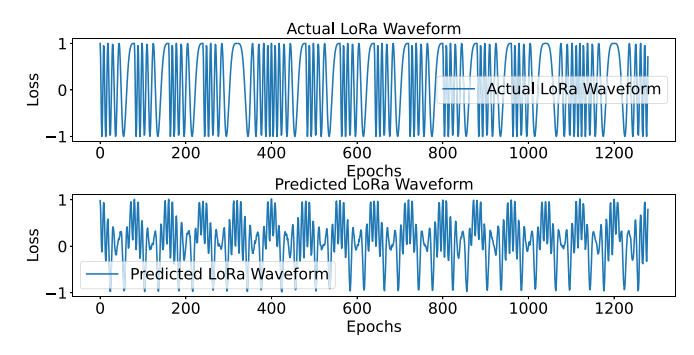


Fig. 14. The predicted LoRa waveform generated by the neural network model after being trained on ZigBee input sequences.

values can achieve higher throughput, as expected, since smaller SF values correspond to faster transmission rates but shorter range. Benchmark systems, corresponding to SF=8, SF=10, and SF=12, show lower throughput than ZigRa at each distance. This indicates that ZigRa offers better performance than the benchmark system across different SF values.

C. LoRa Waveform Generated Via NN

Fig. 14 assess the model's ability to translate ZigBee waveforms to LoRa signals. It shows the predicted LoRa waveform generated by the neural network model after being trained on ZigBee input sequences. The model was trained to predict the LoRa waveform from the corresponding ZigBee signals. This output illustrates how well the neural network can emulate the frequency modulation of LoRa, as learned from the training dataset. The predicted waveform, while similar to the actual one, may exhibit some discrepancies in the frequency sweep, amplitude, or phase, reflecting the model's limitations in perfectly emulating the Chirp Spread Spectrum.

The comparison between the actual and predicted LoRa waveforms helps assess the performance of the neural network. A high degree of similarity between the two signals suggests that the model is successfully learning the underlying characteristics of LoRa modulation from the ZigBee data. However, any noticeable deviations between the two waveforms may indicate areas where the model needs further refinement. These discrepancies could be due to the model's inability to fully capture the subtle features of LoRa's Chirp Spread Spectrum or insufficient training data. Therefore, further improvements in the model's architecture, training data diversity, or training duration might be necessary to enhance the accuracy of the predicted waveforms.

Fig. 15 displays the training and validation loss over the course of the model's training epochs. The training loss represents how well the model is learning to predict the correct LoRa waveforms from the ZigBee input signals during the training process. Ideally, as training progresses, the training loss should decrease, indicating that the model is effectively minimizing the error in its predictions. The validation loss, which is evaluated on a separate validation dataset, is also tracked to ensure that the model is generalizing well and not just overfitting to the training data. If the validation loss remains relatively stable or decreases alongside the training loss, it indicates good generalization.

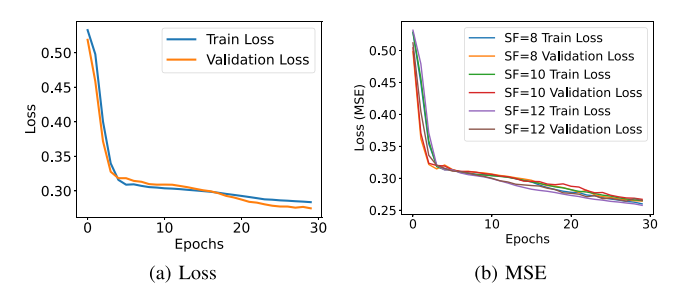


Fig. 15. The training and validation loss over the course of the model's training epochs.

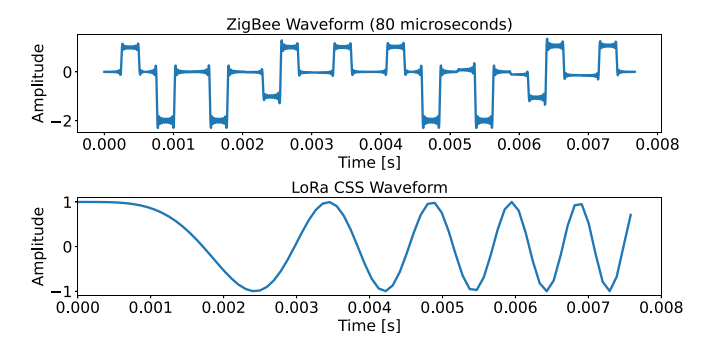


Fig. 16. LoRa Chirp Spread Spectrum (CSS) and the modified ZigBee waveform.

Fig. 15(b) displays the training and validation loss for the model when trained on different SF values, specifically SF=8, SF=10, and SF=12. The training loss represents how well the model is learning from the training data over the epochs, while the validation loss indicates how well the model generalizes to unseen data. As expected, the loss increases as the SF value increases, suggesting that the model struggles more with higher SF values due to the increased complexity of the LoRa signal. For SF=8, the model exhibits the lowest loss, indicating that the waveform is easier for the model to learn and predict. However, as SF increases, the model faces longer symbol durations and more frequency spread, which makes learning more difficult and leads to higher training and validation losses. This trend is typical in sequence-to-sequence tasks where increased input complexity demands more model capacity and longer training time. The higher validation loss for SF=12 also hints at possible overfitting to the training data, as the model may struggle to generalize to the more complex signal structure.

D. Waveform Fitting

Fig. 16 shows the two waveforms-LoRa CSS and the modified ZigBee waveform-are plotted together, with both signals resampled to share a common time axis from 0 to 0.008 seconds. Despite their different modulation schemes, the two waveforms appear quite similar. The LoRa signal exhibits a smooth, continuous frequency change due to its chirp modulation, while the ZigBee waveform, originally a phase-modulated signal, has been adjusted to resemble a frequency-modulated signal. By rescaling the ZigBee waveform's phase shifts to mimic a linear frequency variation, it becomes visually comparable to the LoRa signal.

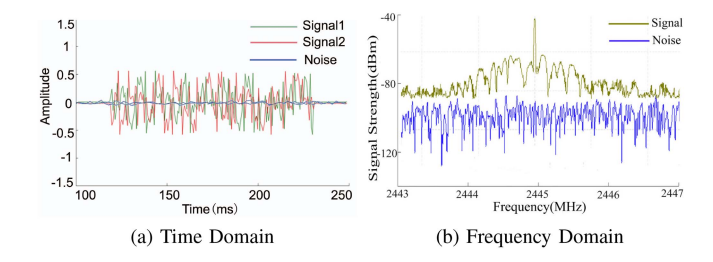


Fig. 17. Long-range real-world communication of ZigRa. (a) Time Domain. (b) Frequency Domain.

Although the ZigBee waveform still retains some of its phase-modulated characteristics, the adjustments made to its symbol durations and resampling process allow the frequency behavior of the ZigBee signal to better match the smooth, continuous change of the LoRa CSS signal. This similarity in waveform appearance indicates that both signals now display a more similar frequency spectrum, despite their underlying differences in modulation technique. This visual alignment highlights how ZigBee's originally discrete frequency shifts can be manipulated to resemble the chirp-like behavior of LoRa.

E. Long Range Communication

Fig. 17 also demonstrates that ZigRa's demodulation technique for ZigBee signals performs nearly as effectively as the LoRa chirp demodulation technique. Specifically, when a chirp and a ZigBee-specific signal are combined and demodulated using FFT with the same FFT size, the resulting magnitudes of the FFT peak are nearly identical, as depicted at the bottom of Fig. 17. Despite being immersed in noise, the weak signal can still be detected and demodulated by the FFT at the LoRa device. This indicates that ZigRa has the potential to achieve receiver sensitivity comparable to LoRa. LoRa is capable of achieving a receiver sensitivity as low as -134 dBm. Consequently, if the Zig-Bee sender transmits a frame at 0 dBm, ZigRa could potentially achieve a link budget of 134 dB. Under ideal conditions, this could result in a theoretical communication distance exceeding 500 meters, though actual range will depend on factors such as path loss, environmental conditions, and antenna characteristics.

F. Outdoor Scenario

To evaluate ZigRa's performance in real-world outdoor environments, we conducted experiments along a campus road, varying the distance between the sender and the receiver from 100 m to 500 m, as illustrated in Fig. 18(a). The experimental settings were carefully chosen, employing a SF and BW of 6 and 1000 kHz, respectively, with a transmission power set to 20 dBm. To compare ZigRa with commodity LoRa, we measured their SERs and PRRs and presented the results in Fig. 18(b) and Fig. 18(c). As the distance between the sender and receiver increased from 100 m to 500 m, ZigRa's SER rose from 0.18 to 0.66, while commodity LoRa's SER increased from 0.15 to 0.58.

Despite ZigRa exhibiting a higher SER due to imperfect emulated signals, it achieved a performance level comparable to (c) PRR

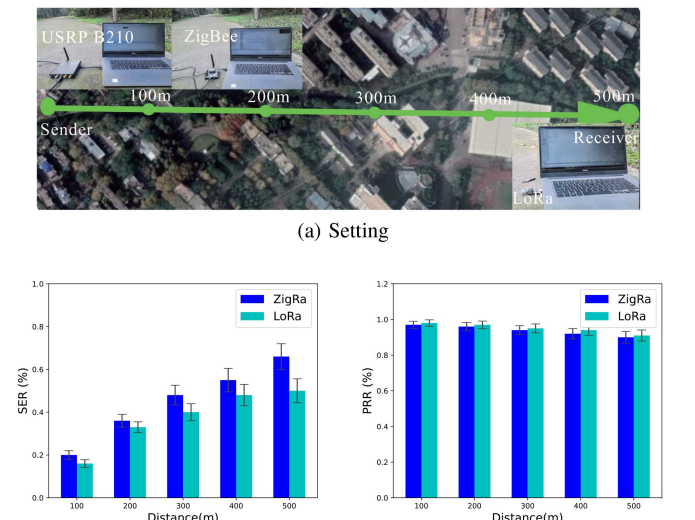


Fig. 18. Long-range real-world performance of ZigRa. (a) Setting. (b) SER. (c) PRR.

(b) SER

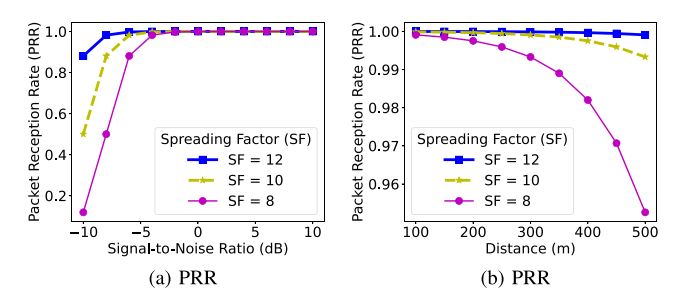


Fig. 19. PRR and SNR and distance for different SFs in the ZigRa communication system. (a) PRR. (b) PRR.

that of commercially available LoRa in terms of both SER and PRR. Therefore, our experimental results effectively demonstrate ZigRa's efficacy within a campus-scale outdoor testbed setting. These findings are particularly relevant for applications requiring dependable and efficient wireless communication over extended distances, such as remote monitoring systems, sensor networks, and smart cities. ZigRa's demonstrated performance establishes it as a viable solution for addressing the communication requirements of such applications, offering reliable connectivity and efficient data transmission capabilities even in challenging outdoor environments.

Fig. 19 illustrates the relationship between PRR and SNR for different SFs in the ZigRa communication system. As the SNR increases, the PRR generally improves for all spreading factors. This is expected because a higher SNR means that the signal strength is stronger relative to the noise, making it easier for the receiver to decode the transmitted packets correctly. The different curves represent the performance for SF=8, SF=10, and SF=12. Generally, a higher spreading factor provides better performance in terms of PRR, especially at lower SNR values. This is because a higher SF increases the robustness of the signal against noise and interference, allowing for more reliable communication even when the SNR is not very high. While higher SFs offer better PRR, they also result in lower data rates

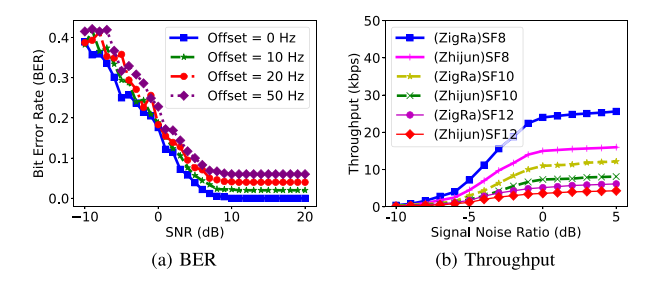


Fig. 20. BER vs. SNR with different frequency offsets. (a) BER. (b) Throughput.

due to the longer duration required for each symbol transmission. This trade-off is evident in the plot, where SF=12 shows the highest PRR but would have the lowest data rate compared to SF=8 and SF=10.

Fig. 19(b) depicts the relationship between PRR and distance for different SFs in the ZigRa communication system. As the distance increases, the PRR generally decreases for all spreading factors. This is expected because the signal strength typically weakens with distance due to factors such as path loss and interference, making it more challenging for the receiver to decode the transmitted packets correctly. The different curves represent the performance for SF=8, SF=10, and SF=12. Generally, a higher spreading factor provides better performance in terms of PRR, especially at longer distances. This is because a higher SF increases the robustness of the signal against noise and interference, allowing for more reliable communication over greater distances.

While higher SFs offer better PRR, they also result in lower data rates due to the longer duration required for each symbol transmission. This trade-off is evident in the plot, where SF=12 shows the highest PRR but would have the lowest data rate compared to SF=8 and SF=10. Our system tolerates minor misalignments by leveraging the FFT demodulation process, which is inherently robust to small time shifts within the chirp window. As demonstrated in Figs. 12 and 19, ZigRa maintains stable performance over varying channel conditions, which include practical timing variations observed in our USRP and commercial chip experiments.

G. Bit Error Rate

Fig. 20 illustrates the BER versus SNR for a communication system experiencing different frequency offsets (0 Hz, 10 Hz, 20 Hz, and 50 Hz). The BER is plotted for each frequency offset at varying SNR values, which reflects how well the system performs under different levels of noise and interference. As the frequency offset increases, the BER tends to increase, especially at lower SNR values. This indicates that higher frequency offsets introduce more distortion in the signal, leading to more bit errors. A 50 Hz offset has the most significant effect, with a noticeably higher BER compared to the other offsets. In contrast, the 0 Hz offset (representing no frequency shift) shows the lowest BER, demonstrating the system's best performance in the absence of frequency misalignment.

As SNR increases, the BER decreases for all frequency offsets, indicating that higher signal quality results in fewer errors. This is typical behavior in communication systems, where stronger signals (higher SNR) enable more accurate data recovery, regardless of the frequency offset. The plot highlights the trade-off between frequency offset and communication reliability. While small offsets (such as 10 Hz or 20 Hz) do not significantly degrade performance at higher SNRs, larger offsets (50 Hz) cause a noticeable increase in error rates, which can be problematic in practical applications. This suggests that frequency synchronization is crucial for minimizing errors, especially in noisy environments.

Fig. 20(b) presents a throughput comparison simulation between the proposed ZigRa system and the systems from references [20], [21] (called the Zhijun system in this comparison). The chart shows throughput (in kbps) at various SNR for different spreading factors (SF=8, SF=10, SF=12). The SNR values range from -10 dB to 5 dB. Each group of bars represents a different spreading factor for both the ZigRa system and the benchmark systems (from [20], [21]). ZigRa (SF=8, SF=10, SF=12): The bars for ZigRa show throughput for the system using different SF. As expected, ZigRa with SF=8 delivers the highest throughput, followed by SF=10 and SF=12, which show progressively lower throughput due to higher redundancy and error correction introduced by the larger spreading factors.

The bars for [20], [21] represent the performance of traditional communication systems, using standard LoRa with fixed spreading factors. The Zhijun system achieves a maximum throughput of around 15 kbps, while Zhijun system performs slightly better, reaching about 18 kbps. These results are consistent across the entire SNR range. As shown in the chart, ZigRa consistently outperforms both systems from [20], [21]. ZigRa with SF=8 achieves the highest throughput, surpassing the Zhijun system by a considerable margin, especially at lower SNR values. This is due to ZigRa's optimized modulation and advanced error correction, which enable more efficient data transmission. We conducted a BER analysis under various frequency offset conditions in Section VI-G (Fig. 20(a)). These results show that ZigRa's demodulation can tolerate offsets up to ± 20 Hz with only modest degradation, and a larger 50Hz offset, although impactful, still maintains BER below 0.3 at moderate SNR. This demonstrates that ZigRa remains operational under realistic oscillator inaccuracies found in commodity ZigBee and LoRa hardware.

H. Practical Deployment on Edge Devices

We clarify that the Transformer model used in ZigRa is applied *offline during a training phase* to construct a mapping table between ZigBee payloads and the resulting LoRa-compatible FFT peaks. Once trained, ZigRa stores a precomputed lookup table of (payload, symbol) pairs. During runtime, the ZigBee device only performs a simple table lookup to select the payload corresponding to the desired LoRa FFT bin.

This table-based approach eliminates the need for Transformer inference on ZigBee hardware altogether. Thus, ZigRa remains fully compatible with commodity ZigBee MCUs (e.g.,

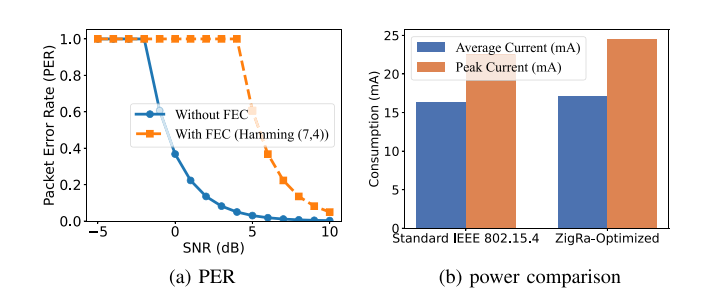


Fig. 21. Packet Error Rate and ZigBee transmitter current consumption. (a) PER. (b) power comparison.

Atmel AT86RF233 or CC2530), which have limited processing and memory budgets (typically tens of KB of RAM and sub-100 MHz CPUs). For completeness, we profiled our Transformer model's inference cost on a representative ARM Cortex-M4 platform (e.g., STM32F4 series with 256 KB RAM and 84 MHz CPU) using TensorFlow Lite Micro. Results indicate: Model size: 32 KB (quantized 8-bit weights). Inference latency: ~1.2 ms for 80-bit input sequences. Memory footprint (stack + heap): <50 KB.

While this is feasible for mid-tier MCUs, in ZigRa's deployment, such inference is not required in the data path. Instead, only a payload_id is transmitted, retrieved from a small static array indexed by desired LoRa symbol index. Therefore, the proposed system architecture ensures that: The learning and optimization happen offline on a server or development host. Runtime payload selection on the ZigBee device involves negligible latency and memory use. No neural model execution is required on the low-end MCU during operation.

I. Packet Error Rate Analysis and Transmitter Power Consumption Analysis

To evaluate the impact of demodulation errors due to FFT peak drift or partial timing misalignment, we analyze ZigRa's packet error rate (PER) under varying SNR, with and without forward error correction (FEC). We use a lightweight (7,4) Hamming code for error correction, encoding every 4 bits into 7 bits at the ZigBee sender before payload selection. The LoRa receiver applies decoding after symbol recovery. Fig. 21(a) shows the PER performance over SNR from -5 to 10 dB. Without FEC, ZigRa begins to experience rapid degradation below 0dB SNR. In contrast, with FEC enabled, the system maintains a PER below 10% down to -2 dB, demonstrating approximately 6 dB of coding gain. This result highlights the feasibility of integrating lightweight FEC into ZigRa to combat residual errors introduced during FFT-based demodulation.

To further evaluate the impact of ZigRa's optimized bit patterns on ZigBee transmitter power consumption, we conducted experiments comparing both standard IEEE 802.15.4 payloads and ZigRa-optimized sequences. As illustrated in Fig. 21(b), two key current metrics-average and peak current—were analyzed to assess the energy efficiency of the transmission process. The average current for standard payloads was measured at 16.3 mA, while the ZigRa variant exhibited a modest increase to 17.1 mA.

Similarly, peak current rose from 22.5 mA to 24.5 mA with ZigRa. This reflects an approximate 9% increase in instantaneous current demand when using ZigRa-enhanced payloads, likely due to reduced DSSS processing gain from the deterministic bit sequences.

VII. RELATED WORK

Physical-layer CTC: Physical-layer CTC technologies, such as WiZig [33] and ZigFi [34], enable direct communication between heterogeneous wireless devices by emulating signals, despite their incompatible physical-layer modulations [30], [31]. This technology acts as a translator, establishing a mutually compatible side channel between two wireless technologies [32]. For example, since WiFi and ZigBee both operate in the 2.4 GHz ISM band, solutions like WEBee [35], TwinBee [36], and Long-Bee [37] can facilitate direct communication between them. CTC simplifies the coordination of heterogeneous wireless devices, even on a shared channel [38]. Several CTC studies propose fulfilling the translation function and support applications such as channel coordination and cross-technology collaboration [39].

WEBee [35] is a software-based PHY-CTC solution that enables direct communication from WiFi to ZigBee. It achieves this by modifying the WiFi transmitter to emulate the ZigBee time-domain waveform, with the WiFi device selecting the payload of a WiFi frame to simulate the ZigBee packet. QAM emulation is at the core of WEBee, which is one example of several PHY-CTC solutions. For instance, XFi [40] enables mobile devices to directly and simultaneously collect data from diverse IoT devices via commodity WiFi radio. XBee [41] is a PHY-CTC solution from ZigBee to BLE, which interprets a ZigBee frame by observing the bit pattern received at the BLE receiver. LEGO-Fi [42] facilitates information transfer from ZigBee to WiFi, alongside numerous others such as WiFi-to-LoRa [43], [44], [45], Bluetooth-to-LoRa [20], [21], Bluetoothto-WiFi [46], LoRa-to-WiFi [47], and LoRa-to-ZigBee [25], [26]. Additional examples can be found in [48], [49], [50], [51], [52] and references therein.

Direct communication between ZigBee and LoRa based on PHY-CTC: LoRaBee [25], [26] was the pioneer in exploring CTC from LoRa to ZigBee in the Sub-1 GHz bands. It facilitated communication from LoRa to ZigBee by embedding specific bytes in the payload of legitimate LoRa packets. These bytes were selected to allow ZigBee devices to recognize the corresponding LoRa chirps by sampling the received signal strength (RSS). LigBee [53] enables symbol-level communication from the latest LPWAN LoRa node to legacy ZigBee nodes. L2X [54] provides long-range CTC to diverse receivers with LoRa transmitters, employing an energy-concentrating demodulation mechanism that de-spreads LoRa chirps over the air. L2X enables non-LoRa receivers to detect and demodulate LoRa signals even under extremely low SNR. Symphony [21] and BLE2LoRa [20] implements a universal LP-WAN on existing heterogeneous wireless devices, enabling concurrent transmission from heterogeneous radios at a Lo-RaWAN device. XiTuXi [55] employ a well-known NMT model called Transformer to learn the bit-sequence to bit-sequence translation rationale behind the CTC without human intervention. S.Kang propose FLEW [56], Unify [57] and DREW [58] for enabling direct communication between WiFi and Bluetooth.

In contrast to previous studies, our work differs from prior research on CTC between LoRa and ZigBee devices in the Sub-1 GHz ISM bands by focusing on the characteristics of LoRa in the 2.4 GHz bands. We introduces a novel approach by leveraging neural networks to perform payload selection at the transmitter. This enables the generation of the required waveform for cross-technology communication. Our approach uses the power of machine learning to dynamically select the appropriate payload that results in the desired waveform for successful communication between LoRa and ZigBee devices in the 2.4 GHz ISM band. By using neural networks, our solution can adapt to various communication scenarios, learning the best parameters for the transmission and ensuring that the generated waveform retains the necessary characteristics for reliable demodulation at the receiver. This provides a more flexible and scalable solution compared to traditional methods, where signal emulation is often rigid and predefined.

VIII. CONCLUSION

In this study, we introduce ZigRa, a novel approach aimed at establishing direct communication from ZigBee devices to LoRa devices. Our investigation involved a thorough analysis of the characteristics of both LoRa and ZigBee networks. Through empirical examinations, we scrutinized LoRa communication from a cross-technology communication perspective, deriving insights to inform the design of ZigRa. ZigRa facilitates longrange cross-technology communication from ZigBee devices to LoRa devices. We conducted extensive experiments to assess ZigRa's performance, and the results underscore its ability to reliably transmit ZigBee communication to LoRa over distances exceeding 500 meters-significantly surpassing the range achievable with native ZigBee communication. Consequently, ZigRa holds promise for addressing applications requiring long-range communication by extending the reach between ZigBee and LoRa networks.

ACKNOWLEDGMENT

The authors are grateful to the anonymous reviewers for their constructive comments in improving the quality of this paper.

REFERENCES

- D. Gao, L. Ou, Y. R. Chen, Y. Liu, and Q. Yang, "ZigRa: Physical-layer cross-technology communication from ZigBee to LoRa," in *Proc. Int. Conf. Wireless Artif. Intell. Comput. Syst. Appl.*, 2024, pp. 114–123.
- [2] W. Wang, X. Liu, Z. Chi, S. Ray, and T. Zhu, "Key establishment for secure asymmetric cross-technology communication," in *Proc. 19th ACM Asia Conf. Comput. Commun. Secur.*, 2024, pp. 412–422.
- [3] D. Xia, X. Zheng, L. Liu, and H. Ma, "Parallel cross-technology transmission from IEEE 802.11 ax to heterogeneous IoT devices," in *Proc. IEEE Conf. Comput. Commun.*, 2023, pp. 1–10.
- [4] Z. Xu et al., "DOFMS: DRL-based out-of-order friendly multipath scheduling in mobile heterogeneous networks," *IEEE Trans. Mobile Com*put., vol. 23, no. 8, pp. 8274–8288, Aug. 2024.

- [5] V. Iyer, V. Talla, B. Kellogg, S. Gollakota, and J. Smith, "Inter-technology backscatter: Towards internet connectivity for implanted devices," in *Proc.* 2016 ACM SIGCOMM Conf., 2016, pp. 356–369.
- [6] W. Wang, S. He, L. Sun, T. Jiang, and Q. Zhang, "Cross-technology communications for heterogeneous IoT devices through artificial doppler shifts," *IEEE Trans. Wireless Commun.*, vol. 18, no. 2, pp. 796–806, Feb. 2019.
- [7] H. Jiang, J. Zhang, X. Guo, and Y. He, "Sense me on the ride: Accurate mobile sensing over a LoRa backscatter channel," in *Proc. 19th ACM Conf. Embedded Networked Sensor Syst.*, 2021, pp. 125–137.
- [8] LoRa Alliance, "Lorawan for developers," 2023. [Online]. Available: https://lora-alliance.org/lorawan-for-developers/
- [9] R. Sharma and R. Arya, "Security threats and measures in the Internet of Things for smart city infrastructure: A state of art," *Trans. Emerg. Telecommun. Technol.*, vol. 34, no. 11, 2023, Art. no. e4571.
- [10] X. Guo et al., "Aloba: Rethinking ON-OFF keying modulation for ambient LoRa backscatter," in *Proc. 18th Conf. Embedded Netw. Sensor Syst.*, 2020, pp. 192–204.
- [11] X. Guo et al., "Saiyan: Design and implementation of a low-power demodulator for LoRa backscatter systems," in *Proc. 19th USENIX Symp. Netw. Syst. Des. Implementation*, 2022, pp. 437–451.
- [12] M. A. Kamal, M. M. Alam, A. A. B. Sajak, and M. M. Su'ud, "Requirements, deployments, and challenges of LoRa technology: A survey," *Comput. Intell. Neurosci.*, vol. 2023, no. 1, vol. 2023, Art. no. 5183062.
- [13] P. Gawłowicz, A. Zubow, and A. Wolisz, "Enabling cross-technology communication between LTE unlicensed and WiFi," in *Proc. IEEE Conf. Comput. Commun.*, 2018, pp. 144–152.
- [14] K. Bhangale, R. Mapari, S. Randive, and K. Mapari, "Cross technology communication between LTE-U and Wi-Fi to improve overall QoS of 5G system," in *Proc. 2nd Asian Conf. Innov. Technol.*, 2022, pp. 1–6.
- [15] X. Limani, H. C. C. De Resende, V. Charpentier, J. Marquez-Barja, and R. Riggio, "Enabling cross-technology communication to protect vulnerable road users," in *Proc. IEEE Conf. Netw. Funct. Virtualization Softw. Defined Netw.*, 2022, pp. 39–44.
- [16] Y. He, J. Guo, and X. Zheng, "From surveillance to digital twin: Challenges and recent advances of signal processing for industrial Internet of Things," *IEEE Signal Process. Mag.*, vol. 35, no. 5, pp. 120–129, Sep. 2018.
- [17] S. Wang et al., "X-disco: Cross-technology neighbor discovery," in Proc. 19th Annu. IEEE Int. Conf. Sens., Commun., Netw., 2022, pp. 163–171.
- [18] Y. He et al., "Cross-technology communication for the Internet of Things: A survey," ACM Comput. Surv., vol. 55, no. 5, pp. 1–29, 2022.
- [19] Z. Chi, Y. Li, H. Sun, Z. Huang, and T. Zhu, "Simultaneous bi-directional communications and data forwarding using a single ZigBee data stream," *IEEE/ACM Trans. Netw.*, vol. 29, no. 2, pp. 821–833, Apr. 2021.
- [20] Z. Li and Y. Chen, "BLE2LoRa: Cross-technology communication from bluetooth to LoRa via chirp emulation," in *Proc. 17th Annu. IEEE Int. Conf. Sens.*, *Commun.*, *Netw.*, 2020, pp. 1–9.
- [21] Z. Li and Y. Chen, "Achieving universal low-power wide-area networks on existing wireless devices," in *Proc. IEEE 27th Int. Conf. Netw. Protoc.*, 2019, pp. 1–11.
- [22] J. Yan, S. Cheng, Z. Li, and J. Liu, "PCTC: Parallel cross technology communication in heterogeneous wireless systems," in *Proc. 21st ACM/IEEE Int. Conf. Inf. Process. Sensor Netw.*, 2022, pp. 67–78.
- [23] Texas Instruments LAUNCHXL-CC1352R1, "SimpleLink multi-band CC1352R wireless MCU launchpad development Ki," Jun. 28, 2025. [Online]. Available: https://www.ti.com/tool/LAUNCHXL-CC1352R1
- [24] Z. Sun, H. Yang, K. Liu, Z. Yin, Z. Li, and W. Xu, "Recent advances in LoRa: A comprehensive survey," ACM Trans. Sensor Netw., vol. 18, no. 4, pp. 1–44, 2022.
- [25] J. Shi, D. Mu, and M. Sha, "LoRaBee: Cross-technology communication from LoRa to ZigBee via payload encoding," in *Proc. IEEE 27th Int. Conf. Netw. Protoc.*, 2019, pp. 1–11.
- [26] J. Shi, D. Mu, and M. Sha, "Enabling cross-technology communication from LoRa to ZigBee via payload encoding in Sub-1 GHz Bands," ACM Trans. Sensor Netw., vol. 18, no. 1, pp. 1–26, 2021.
- [27] P. Gawlowicz, A. Zubow, and F. Dressler, "Wi-Lo: Emulation of LoRa using Commodity 802.11b WiFi Devices," in *Proc. IEEE Int. Conf. Commun.*, 2022, pp. 4414–4419.
- [28] L. Vangelista, "Frequency shift chirp modulation: The LoRa modulation," IEEE Signal Process. Lett., vol. 24, no. 12, pp. 1818–1821, Dec. 2017.
- [29] EPFL, "LoRa PHY based on GNU radio," 2023. [Online]. Available: https://www.epfl.ch/labs/tcl/resources-and-sw/lora-phy/
- [30] S. Wang, Z. Yin, Z. Li, Y. Chen, S. M. Kim, and T. He, "Networking support for bidirectional cross-technology communication," *IEEE Trans. Mobile Comput.*, vol. 20, no. 1, pp. 204–216, Jan. 2021.

- [31] S. Oh et al., "Supporting flexible and transparent user interface distribution across mobile devices," *IEEE Trans. Mobile Comput.*, vol. 23, no. 8, pp. 8398–8417, Aug. 2024.
- [32] J. Yao, H. Huang, J. Su, R. Xie, X. Zheng, and K. Wu, "Enabling cross-technology coexistence for ZigBee devices through payload encoding," *IEEE Trans. Mobile Comput.*, vol. 23, no. 8, pp. 8289–8306, Aug. 2024.
- [33] X. Guo, Y. He, and X. Zheng, "WIZig: Cross-technology energy communication over a noisy channel," *IEEE/ACM Trans. Netw.*, vol. 28, no. 6, pp. 2449–2460, Dec. 2020.
- [34] X. Guo, Y. He, X. Zheng, L. Yu, and O. Gnawali, "ZIGFI: Harnessing channel state information for cross-technology communication," *IEEE/ACM Trans. Netw.*, vol. 28, no. 1, pp. 301–311, Feb. 2020.
- [35] Z. Li and T. He, "WeBee: Physical-layer cross-technology communication via emulation," in *Proc. 23rd Annu. Int. Conf. Mobile Comput. Netw.*, 2017, pp. 2–14.
- [36] Y. Chen, Z. Li, and T. He, "TwinBee: Reliable physical-layer cross-technology communication with symbol-level coding," in *Proc. IEEE Conf. Comput. Commun.*, 2018, pp. 153–161.
- [37] Z. Li and T. He, "LongBee: Enabling long-range cross-technology communication," in *Proc. IEEE Conf. Comput. Commun.*, 2018, pp. 162–170.
- [38] B. Sheng, R. Han, H. Cai, F. Xiao, L. Gui, and Z. Guo, "CDFI: Cross-domain action recognition using WiFi signals," *IEEE Trans. Mobile Comput.*, vol. 23, no. 8, pp. 8463–8477, Aug. 2024.
- [39] D. Gao et al., "LoBee: Bidirectional communication between LoRa and ZigBee based on physical-layer CTC," *IEEE Trans. Wireless Commun.*, early access, Apr. 08, 2025, doi: 10.1109/TWC.2025.3556552.
- [40] R. Liu, Z. Yin, W. Jiang, and T. He, "XFI: Cross-technology IoT data collection via commodity WiFi," in *Proc. IEEE 28th Int. Conf. Netw. Protoc.*, 2020, pp. 1–11.
- [41] W. Jiang, S. M. Kim, Z. Li, and T. He, "Achieving receiver-side cross-technology communication with cross-decoding," in *Proc. 24th Annu. Int. Conf. Mobile Comput. Netw.*, 2018, pp. 639–652.
- [42] X. Guo, Y. He, X. Zheng, Z. Yu, and Y. Liu, "Lego-FI: Transmitter-transparent CTC with cross-demapping," *IEEE Internet Things J.*, vol. 8 no. 8, pp. 6665–6676, Apr. 2021.
- [43] D. Xia, X. Zheng, F. Yu, L. Liu, and H. Ma, "WiRa: Enabling cross-technology communication from WiFi to LoRa with IEEE 802.11 ax," in *Proc. IEEE Conf. Comput. Commun.*, 2022, pp. 430–439.
- [44] X. Zheng, D. Xia, F. Yu, L. Liu, and H. Ma, "Enabling cross-technology communication from WiFi to LoRa with IEEE 802.11ax," *IEEE/ACM Trans. Netw.*, vol. 32, no. 3, pp. 1936–1950, Jun. 2024.
- [45] D. Gao et al., "WiLo: Long-range cross-technology communication from Wi-Fi to LoRa," *IEEE Trans. Commun.*, vol. 73, no. 3, pp. 1677–1691, Mar. 2025, doi: 10.1109/TCOMM.2024.3461574.
- [46] D. Gao et al., "Physical-layer CTC from BLE to Wi-Fi with IEEE 802.11ax," IEEE Trans. Mobile Comput., vol. 24, no. 1, pp. 338–351, Jan. 2025.
- [47] D. Gao, W. Jiang, W. Wang, Z. Han, and Y. Liu, "LoFi: Physical-layer CTC from LoRa to WiFi with IEEE 802.11ax," in *Proc. IEEE Int. Conf. Comput. Commun.*, 2025, pp. 1–10.
- [48] T. Cheng, S. Li, F. Jiao, and Y. Pan, "WibZig: Reliable and commodity-device compatible PHY-CTC via chip emulation in phase," in *Proc. 22nd Int. Conf. Inf. Process. Sensor Netw.*, 2023, pp. 191–204.
- [49] W. Wang et al., "Simultaneous data dissemination among WiFi and Zig-Bee devices," *IEEE/ACM Trans. Netw.*, vol. 31, no. 6, pp. 2545–2558, Dec. 2023.
- [50] J. Wang, W. Jiang, R. Liu, B. Hu, D. Gao, and S. Wang, "NN-Defined modulator: Reconfigurable and portable software modulator on IoT gateways," in *Proc. 21st USENIX symp. Netw. Syst. Des. Implementation*, 2024, pp. 775–789.
- [51] S. Yao, X. Xu, H. Chen, Y. Sun, and Q. Zhao, "Deep joint source-channel coding for efficient and reliable cross-technology communication," in *Proc. IEEE Int. Conf. Commun.*, 2024, pp. 3524–3529.
- [52] D. Xia, X. Zheng, L. Liu, C. Wang, and H. Ma, "c-Chirp: Towards symmetric cross-technology communication over asymmetric channels," *IEEE/ACM Trans. Netw.*, vol. 29, no. 3, pp. 1169–1182, Jun. 2021.
- [53] Z. Wang et al., "LigBee: Symbol-level cross-technology communication from LoRa to ZigBee," in *Proc. IEEE Conf. Comput. Commun.*, 2023, pp. 1–10.
- [54] S. Tong, Y. He, Y. Liu, and J. Wang, "De-spreading over the air: Long-range CTC for diverse receivers with LoRa," in *Proc. 28th Annu. Int. Conf. Mobile Comput. Netw.*, 2022, pp. 42–54.
- [55] S. Liao, Z. An, Q. Pan, X. Zhao, J. Tong, and L. Yang, "XiTuXi: Sealing the gaps in cross-technology communication by neural machine translation," in *Proc. 21st ACM Conf. Embedded Netw. Sensor Syst.*, 2023, pp. 70–82.

- [56] W. Hsun, S. Cho, and G. Kang, "FLEW: Fully emulated WiFi[C]," in Proc. 28th Annu. Int. Conf. Mobile Comput. And Netw., 2022, pp. 29–41.
- [57] H.-W. Cho and K. G Shin, "Unify: Turning BLE/FSK SoC into WiFi SoC," in Proc. 29th Annu. Int. Conf. Mobile Comput. Netw., 2023, pp. 1–15.
- [58] H.-W. Cho and K. G. Shin1, "DREW: Double-throughput emulated WiFi," in *Proc. 30th Annu. Int. Conf. Mobile Comput. Netw.*, 2024, pp. 663–678.



Demin Gao (Member, IEEE) received the PhD degree from the Department of Computer Science and Engineering, Nanjing University of Science and Technology, Nanjing, China, in 2012. During 2011–2012, he studied as a joint PhD degree student and has attended the Research Lab of Kwan-wu Chin with School of Electrical, Computer Telecommunications Engineering, University of Wollongong, Australia. He joined the College of Information Science and Technology, Nanjing Forestry University, China, as a lecturer and an associate professor in 2012 and

2016, respectively. During 2013–2016, he was with the School of Computer Science and Engineering, Southeast University, Nanjing City, China, where he was working toward the advanced postdoctoral engineering training. In 2016, he was a visiting scholar to work toward his research and attended the Research Lab of Tian He with the Department of Computer Science and Engineering, University of Minnesota Twin Cities, Minneapolis, MN, USA.



Yongrui Chen (Member, IEEE) received the MS degree from Tsinghua University, China, in 2007, and the PhD degree from University of Chinese Academy of Sciences, China, in 2011. He is currently an associate professor with the School of Electronic, Electrical and Communication Engineering, University of Chinese Academy of Sciences. His research interests include Internet of Things, wireless and mobile computing, and heterogeneous wireless networks. He is an member of IEEE.



Ye Liu (Senior Member, IEEE) received the MS and PhD degrees in electronic science and engineering from Southeast University, Nanjing, China, in 2013 and 2018, respectively. From 2014 to 2015, he was a visiting scholar with Montana State University, Bozeman, MT, USA. From 2017 to 2018, he was a joint PhD student with Networked Embedded Systems Group, RISE Swedish Institute of Computer Science, Kista, Sweden. He is currently an associate professor with Nanjing Agricultural University, Nanjing. He has authored or coauthored papers in

several prestigious journals, such as the IEEE Communications Magazine, IEEE Wireless Communications, IEEE Internet of Things Journal, ACM Transactions on Embedded Computing System, and IEEE Network. His research interests include the Internet of Things, energy harvesting, and tiny machine learning. Dr. Liu was the recipient of the 1st place of the EWSN Dependability Competition in 2019.



Hongang Wang (Fellow, IEEE) is currently the founding chair and professor with the Department of Graduate Computer Science and Engineering, Katz School of Science and Health, Yeshiva University, New York, NY, USA. He was a professor with UMass Dartmouth (UMassD). He is also an alumnus with NAE Frontiers of Engineering Program. He has graduated 30 MS/PhD degree students and has produced high-quality publications in prestigious journals and conferences in his research areas, winning several prestigious Best Paper awards. His research interests

include Internet of Things and its applications in health and transportation (e.g., autonomous vehicles) domains, machine learning and Big Data, multimedia and cyber security, smart and connected health, wireless networks, and multimedia communications. During 2020–2022, he was the Editor in Chief (EiC) of *IEEE Internet of Things Journal*. From 2018 to 2020, he was the past chair of IEEE Multimedia Communications Technical Committee and the past IEEE eHealth Technical Committee Chair from 2020 to 2021. He is an IEEE distinguished lecturer and a fellow of AAIA.